Journal of Materials Chemistry B

PAPER

View Article Online
View Journal | View Issue

Cite this: J. Mater. Chem. B, 2015, 3, 3490

Coumarin–benzothiazole–chlorambucil (Cou–Benz–Cbl) conjugate: an ESIPT based pH sensitive photoresponsive drug delivery system†

Shrabani Barman,[a] Sourav K. Mukhopadhyay,[b] Moumita Gangopadhyay,[a] Sandipan Biswas,[a] Satyahari Dey*[b] and N. D. Pradeep Singh*[a]

Received 17th December 2014,
Accepted 12th March 2015

DOI: 10.1039/c4tb02081b

www.rsc.org/MaterialsB

We have developed an ESIPT based drug delivery system (DDS), Cou–Benz–Cbl conjugate, by incorporating a benzothiazole group at the 8th position of the 7-hydroxy-coumarin moiety for pH sensitive fluorescence properties and photocontrolled release of the anticancer drug chlorambucil. The Cou–Benz–Cbl conjugate exhibited unique photophysical properties like good absorbance at around 350 nm, a large Stokes shift (~151 nm) and pH sensitive fluorescence properties. The pH sensitive fluorescence properties of the Cou–Benz–Cbl conjugate can be ascribed to an ESIPT turn "on and off" mechanism. At physiological pH, the ESIPT gets turned "off" and a blue fluorescence of the coumarin moiety was observed, but at acidic pH, the ESIPT gets turned "on" and a green fluorescence was noted. Photolysis of the Cou–Benz–Cbl conjugate using UV light of wavelength ≥365 nm resulted in the efficient release of the anticancer drug chlorambucil. Cellular uptake studies revealed that the Cou–Benz–Cbl conjugate was easily internalized inside the cancer cells. Further, an MTT assay showed that the Cou–Benz–Cbl conjugate has a good biocompatibility and low cytotoxicity towards the MDA-MB-231 cell line, whereas upon exposure to UV light, the Cou–Benz–Cbl conjugate exhibited enhanced cytotoxicity compared to the free drug due to the effective release of the anticancer drug chlorambucil inside the cancer cell.

Introduction

Photoresponsive drug delivery systems (DDSs) have recently received much attention for their applications, especially in the area of cancer treatment, since they allow precise control over the release, including the location, timing and dosage.[1,2] One of the main ingredients used for the construction of photoresponsive DDSs is a phototrigger. Several phototriggers have been reported so far in the literature. Among them, coumarin derivatives have been widely used in DDSs mainly due to their strong fluorescence nature and faster release ability. However, coumarin based phototriggers still face disadvantages like a small Stokes shift resulting in self-absorption (inner-filter effects),[3] an enhancement of the signal to noise ratio in bioimaging applications,[4] and fluorescence properties which are insensitive to the intracellular pH environment.[5] Such kinds of limitations prevent coumarin based phototriggers from broad acceptance in the areas of cell imaging and drug delivery. As a result, several chemical modifications of these coumarin phototriggers have been attempted to overcome the above mentioned limitations, but their synthesis remains a challenging task.

Recently, excited state intramolecular proton transfer (ESIPT) has attracted great attention due to its applications in major areas like laser dyes,[6] photostabilisers,[7] radiation scintillators,[8] luminescent materials,[9] molecular probes,[10] sensing ions,[11–14] and photoswitching of polymorphs.[15] Most of the ESIPT reactions involve enol–keto photo-tautomerisation[16] in the excited state of the ESIPT molecule leading to an initial enol form and a photo-tautomer keto form. As a result, this gives rise to dual fluorescence, one originating from the enol form and another largely red shifted fluorescence from the tautomeric keto form in the excited state. In particular, the emission maximum and the fluorescence quantum yield of the enol and tautomeric keto forms are highly sensitive to the environment conditions, like pH,[17] solvent,[18] *etc.* The above characteristic features, like a large Stokes shift and environmentally sensitive fluorescence properties, of ESIPT molecules

[a] Department of Chemistry, Indian Institute of Technology, Kharagpur 721302, West Bengal, India. E-mail: ndpradeep@chem.iitkgp.ernet.in
[b] Department of Biotechnology, Indian Institute of Technology, Kharagpur 721302, West Bengal, India

† Electronic supplementary information (ESI) available: General experimental procedures, characterization of compounds **3**, $\mathbf{C_4}$ and $\mathbf{C_5}$, the naked eye color of a solution of $\mathbf{C_5}$ in different solvents, the naked eye color of a solution of $\mathbf{C_5}$ in different solvents under a fluorescent lamp, fluorescence quantum yield calculations of $\mathbf{C_4}$, $\mathbf{C_5}$ and 4-methyl-7-hydroxycoumarin, fluorescence lifetime calculations of $\mathbf{C_5}$ and $\mathbf{C_4}$ in different solvents (λ_{max} = 516 nm and λ_{max} = 406 nm), time-resolved decay curves of $\mathbf{C_5}$ and $\mathbf{C_4}$ in different solvents (λ_{max} = 516 nm and λ_{max} = 406 nm), photochemical quantum yield calculation of $\mathbf{C_5}$. See DOI: 10.1039/c4tb02081b

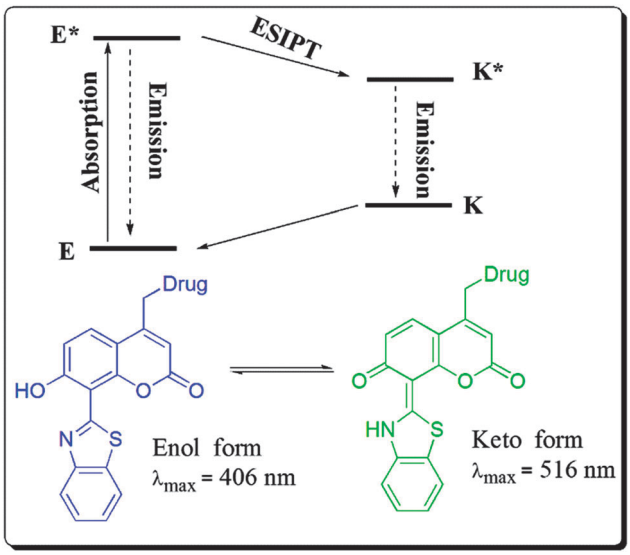

Scheme 1 ESIPT process: enol and keto forms of the DDS.

encouraged us to utilize them for the first time in the design of a pH sensitive coumarin based photoresponsive DDS.

Among the various ESIPT molecules, 2-(2′-hydroxyphenyl)-benzothiazole (HBT) is a compound of interest due to its interesting properties, such as (i) its simple structure, (ii) its facile chemical modification, and (iii) the large Stokes shift arising from excited-state intramolecular proton transfer (ESIPT).[19] In addition, the HBT molecule also shows dual emission, which is highly dependent on the solution pH[20] and proticity.[21] As a result, HBT is utilized in various applications including chemical sensors,[22] OLEDs,[23] laser dyes,[24] polymer modifiers[25] and polymeric materials.[26]

Hence, we thought about incorporating the HBT molecule with the 7-hydroxy coumarin phototrigger so that we can have a DDS with a larger Stokes shift[27] and pH sensitive fluorescence properties.[28] The pH sensitive fluorescence properties of the DDS can be ascribed to an ESIPT "on and off" mechanism. At physiological pH, the ESIPT will be switched "off" (deprotonation of the 7-hydroxy group in coumarin will occur since the pH of the coumarin phenolic –OH group is 6.8) and a blue fluorescence of the coumarin moiety will be observed, but at acidic pH, the ESIPT will be turned "on" and we can observe a green fluorescence from the tautomeric keto form resulting from the intramolecular proton transfer (Scheme 1). Further, we wanted to incorporate a benzothiazole group at the 8th position of the coumarin moiety so that the H-chelated ring forming distance between the H-donor (7-hydroxy group of the coumarin moiety) and the acceptor (nitrogen atom of HBT) are at the optimum distance.[29] Keeping this in mind for the current study, we have synthesized a new pH sensitive benzothiazole–coumarin based photoresponsive DDS for the delivery of the anticancer drug chlorambucil.

Experimental

Synthesis of Cou–Benz–Cbl conjugate (DDS)

8-Formyl-7-hydroxyl-4-(hydroxymethyl)-coumarin (3). 7-Hydroxy-4-(hydroxymethyl)-coumarin (1 equiv.) and hexamine (4 equiv.) in trifluoroacetic acid (TFA) were refluxed for 2 h. After cooling, the reaction mixture was extracted with dichloromethane (DCM), and the combined organic layers were dried over $MgSO_4$ and evaporated under reduced pressure. A pale yellow solid of 8-formyl-7-hydroxy-4-(hydroxymethyl)-coumarin was obtained. The crude material was purified by column chromatography through silica gel using EtOAc/petroleum ether (2 : 8) to obtain a light yellow powder (yield 20%); mp: 180–182 °C; ^{1}H NMR ($CDCl_3$, 200 MHz): δ = 12.27 (s, 1H), 10.63 (s, 1H), 8.24 (s, 1H), 7.68–7.63 (d, J = 9.2 Hz, 1H), 6.96–6.92 (d, J = 9.2 Hz, 1H), 6.45 (s, 1H), 5.35 (s, 1H); ^{13}C NMR ($CDCl_3$, 50 MHz): δ = 193.1 (1C), 165.5 (1C), 159.7 (1C), 158.6 (1C), 148.3 (1C), 131.7 (1C), 130.6 (1C), 114.8 (1C), 110.7 (1C), 108.9 (1C), 60.4 (1C); FTIR (KBr, cm^{-1}): 3210, 2800, 1756, 1703; MS cal. for $C_{11}H_9O_5$ [MH^+]: 221.0450, found: 221.0441.

8-Benzothiazoyl-7-hydroxyl-4-(hydroxymethyl)-coumarin (Cou–Benz–OH) (C_4). A mixture of 8-formyl-7-hydroxy-4-(hydroxymethyl)-coumarin (1 equiv.) and *o*-amino-thiophenol (1 equiv.) in dry DMSO was refluxed for 1 h. After cooling, the reaction mixture was extracted with ethyl acetate (10 × 3 = 30 mL). The combined organic layers were dried over $MgSO_4$ and evaporated under reduced pressure. A pale yellow solid of 8-benzothiazoyl-7-hydroxy-4-(hydroxymethyl)-coumarin (C_4) was obtained. The crude material was purified by column chromatography through silica gel using EtOAc/petroleum ether (3 : 7) to obtain an off white powder (yield 50%); mp: >200 °C; ^{1}H NMR (DMSO-d_6, 200 MHz): δ = 14.43 (bs, –OH), 8.48–8.44 (dd, J = 8 Hz, 1H), 8.34–8.31 (dd, J = 7.4 Hz, 1H), 8.22–8.18 (d, J = 8.4 Hz, 1H), 7.67–7.52 (m, 2H), 7.12–7.10 (d, J = 8.8 Hz, 1H), 6.41 (s, 1H), 4.8 (s, 2H); ^{13}C NMR (DMSO-d_6, 50 MHz): δ = 162.9 (1C), 161.4 (1C), 158.9 (1C), 157.3 (1C), 151.8 (1C), 148.4 (1C), 133.0 (1C), 128.0 (1C), 127.1 (1C), 125.9 (1C), 124.2 (1C), 122.1 (1C), 121.6 (1C), 114.0 (1C), 109.3 (1C), 106.6 (1C), 59.2 (1C); FTIR (KBr, cm^{-1}): 3250 (broad), 1754, 1703; MS cal. for $C_{17}H_{12}NO_4S$ [MH^+]: 326.0487, found: 326.0498.

Coumarin–benzothiazoyl–chlorambucil conjugate (Cou–Benz–Cbl) (C_5). Chlorambucil (1 equiv.) was dissolved in 1 mL of oxalyl chloride and was stirred for 1 h at 60 °C. Then, the oxalyl chloride was removed under vacuum to afford the acid chloride of chlorambucil as a brown oil. Then, the acid chloride was dissolved in dry DMF (5 mL) and the esterification reaction was carried out without further purification. To the solution of the acid chloride in DMF (5 mL), C_4 (1.2 equiv.) was added, followed by triethylamine (62 μL, 0.45 mmol). The mixture was stirred at 55 °C for 8 h. After cooling, the reaction mixture was extracted with ethyl acetate (10 × 3 = 30 mL). The combined organic layers were dried over $MgSO_4$ and evaporated under reduced pressure. A pale yellow solid of C_5 was obtained. The crude material was purified by column chromatography through silica gel using EtOAc/petroleum ether (2 : 8) to obtain a white solid (yield 90%); mp: >200 °C; ^{1}H NMR ($CDCl_3$, 200 MHz): δ = 8.09–7.99 (m, 2H), 7.61–7.48 (m, 3H), 7.36 (s, 1H), 7.13–7.12 (d, J = 3 Hz, 1H), 7.09–7.07 (d, J = 3.4 Hz, 1H), 6.81–6.76 (d, J = 8.6 Hz, 2H), 6.4 (s, 1H), 5.3 (s, 2H), 3.74–3.61 (m, 8H), 2.66–2.59 (t, J = 6.6 Hz, 2H), 2.52–2.44 (t, J = 7.4 Hz, 2H), 2.07–1.96 (m, 2H); ^{13}C NMR (DMSO-d_6, 50 MHz): δ = 175.1 (1C), 163.6 (1C), 162.1 (1C), 159.7 (1C), 158.0

(1C), 152.5 (1C), 149.1(1C), 145.1 (1C), 133.8 (1C), 130.4 (1C), 130.0 (2C), 126.6 (1C), 125.2 (1C), 124.8 (1C), 122.8 (1C), 122.3 (1C), 114.7 (1C), 112.6 (2C), 110.0 (1C), 107.3 (1C), 105.8 (1C), 59.9 (1C), 52.9 (2C), 41.8 (2C), 33.7 (1C), 27.2 (1C), 22.7 (1C); FTIR (KBr, cm^{-1}): 3250 (broad), 1754, 1710; MS cal. for $C_{31}H_{29}C_{l2}N_2O_5S$ $[MH^+]$: 611.1174, found: 611.1155.

Photophysical properties of C_5. The absorption and emission spectra of a degassed solution of C_5 (2×10^{-5} M) in different solvents were recorded on a UV-vis spectrophotometer and fluorescence spectrophotometer, respectively.

Photolysis of C_5 using soft UV irradiation ($\geq$365 nm). C_5 (1 mg) was dissolved in a methanol/water (1 : 1 v/v, 1 mL) mixture. Half of the solution was kept in the dark and the remaining half was purged with nitrogen and irradiated under UV light ($\geq$365 nm, 125 W medium pressure Hg lamp) using a suitable filter (1 M $CuSO_4$ solution in 0.1 N H_2SO_4). At periodic time intervals, a small aliquot (100 μL) of the solution was taken out and analyzed by RP-HPLC using a mobile phase of methanol/water (8 : 2 v/v) at a flow rate of 0.5 mL min^{-1}.

Antiproliferative activity assays

Cell lines. Human breast carcinoma (MDA-MB-231) was obtained from the National Centre for Cell Science (NCCS), Pune, India and maintained in Dulbecco's Modified Eagle's Medium (DMEM) medium supplemented with 10% fetal bovine serum. The cells were cultured at 37 °C in a CO_2 incubator (Thermo Fisher Scientific, USA).

Real time cellular uptake and localization studies. To study the cellular uptake and localization of C_5, MDA-MB-231 cells were first seeded at a density of 1×10^5 cells per well in a 6 well plate and then incubated with 10 μg mL^{-1} of C_5 for 4 h at 37 °C in a CO_2 incubator. After incubation, the cells were irradiated with UV light ($\geq$365 nm) using a UV lamp (Bangalore Genei Pvt. Ltd) for 0–30 min. Thereafter, the cells were fixed using 4% paraformaldehyde for 10 min and washed twice with PBS. Imaging was done using confocal microscopy (CLSM; Olympus FV 1000 attached to an inverted microscope 1X81, Japan).

In vitro cytotoxicity assay

Before irradiation. The cytotoxicity of C_4, C_5 and chlorambucil (Cbl) were determined with and without UV irradiation on MDA-MB-231 cells using an MTT assay according to the method by Mosmann.[30] The breast cancer cells (1×10^5 cells per well of a 96 well plate) were treated for 48 h with different concentrations (0.1–10 μg mL^{-1}) and the cell viability was determined by an MTT assay (Mosmann, 1983),[30] measuring the absorbance at 595 nm using a micro plate reader (Bio-Rad 550). The cell viability was calculated using the formula: viability (%) = $100 \times A_2/A_1$, where A_2 is the absorbance of the treated cells and A_1 is the absorbance of the control cells.

After irradiation. The breast cancer cells (1×10^5 cells per well of a 96 well plate) were treated with different concentrations of C_4, C_5 and Cbl (0.1–10 μg mL^{-1}) and incubated for 4 h at 37 °C in a CO_2 incubator. Thereafter, the cells were irradiated with UV light ($\lambda \geq 365$ nm) for 30 min (keeping the culture plate 6 cm from the light source) using a UV lamp (Bangalore Genei Pvt. Ltd) under aseptic conditions. After UV irradiation, the cells were again incubated for 48 h and the cell viability was measured by an MTT assay (Mosmann, 1983).[30] The cell viability was calculated as described above.

Real time drug release *in vitro* and cytotoxicity

The cytotoxicity of the time dependent controlled released drug with irradiation on the MDA-MB-231 cell line was determined by a conventional MTT assay (Mosmann, 1983).[30] Briefly, the cells in the exponential growth phase were trypsinised and seeded in 96 well culture plates (1×10^5 cells per well). After 12 h of cell seeding, the medium was replaced with fresh complete medium (DMEM) containing 10 μg mL^{-1} of C_5 and this was kept for 4 h at 37 °C in a CO_2 incubator. The drug treated cells were irradiated with UV-light ($\geq$365 nm) for 0–30 min. The assay was performed in triplicate for each time frame (0, 5, 10, 15, 20, 25 and 30 min). Then, the plate was further incubated for 48 h at 37 °C in a CO_2 incubator. The real time drug released *in vitro* was measured spectrophotometrically in accordance with measuring the cell viability by the MTT assay.

Fluorescence microscopy

The real time drug release from C_5 after UV-irradiation ($\geq$365 nm) was also studied by fluorescence microscopy. MDA-MB-231 cells (1×10^5 cells per well) were treated with 10 μg mL^{-1} of C_5 and put aside for 4 h at 37 °C. Then, the drug treated cells were irradiated with UV-light ($\geq$365 nm) for 0–30 min. Thereafter, the plate was incubated for 48 h at 37 °C in a CO_2 incubator. The effect of the released drug on the cell was visually observed by fluorescence microscopy (1X51, Olympus) and a high-performance CCD camera with an appropriate filter using Image-Pro Discovery 5.1 software.

Cell cycle analysis

The cell cycle distributions of the cells (with and without drug treatment) were analyzed by propidium iodide (PI) DNA staining, according to the method by Pilatova *et al.*[31] Briefly, the MDA-MB-231 cells (1×10^6) after C_5 (10 μg mL^{-1}) treatment, UV irradiation (30 min) and incubation for 48 h were harvested for cell cycle analysis by flow cytometry. The cells were washed twice with PBS (pH 7.4) and fixed overnight in 70% ethanol at −20 °C. Then, the cells were washed with phosphate buffered saline (PBS), followed by incubation with 1 mg mL^{-1} RNase A and 10 μg mL^{-1} propidium iodide at 37 °C. Ten thousand cells were counted per analysis. PI fluorescence was detected in the pulse-processed FL2 channel. The distributions of cells in the different cell cycle phases were analyzed from the DNA histogram using a Becton-Dickinson FACSCalibur flow cytometer and CellQuest™ pro software. The percentage of cells corresponding to sub G0/G1, G0/G1, S and G2/M phases of the cell cycle were analyzed from the DNA histogram. A sub-G0/G1 fraction of cells was identified as an apoptosis population.

Apoptosis detection by SEM

MDA-MB-231 cells (1×10^5) were seeded on sterile cover slips, placed in a 6 well plate and incubated overnight for cell attachment. Then, the cells were treated with 10 μg mL^{-1} of C_5, irradiated with UV-light as described earlier and finally incubated for 48 h. The cells were further washed with PBS and fixed with 4% paraformaldehyde. Thereafter, the cells were again washed twice with PBS and dehydrated in various grades of ethanol (30–100%). Then, the samples were dried in desiccators. Samples were then fixed onto a graphite stub and kept in an auto sputter coater (E5200, Bio-Rad) under vacuum for up to 150 s for gold coating. Images were captured using a field emission scanning electron microscope (FESEM) from Carl Zeiss (model SUPRATM 40) with an accelerated voltage of 5–20 kV.[34]

Nuclear morphology determination by PI staining

The assay was performed as described previously by Shon *et al.*[32] Briefly, 1×10^5 MDA-MB-231 cells after C_5 treatment (both UV non-irradiated and irradiated) for 48 h were rinsed twice with PBS and fixed in 4% formaldehyde solution for 10 min. Thereafter, the cells were washed with PBS and permeabilized with 0.1% Triton-X. The cells were again washed with PBS and stained with PI (10 μg mL^{-1}) under dark conditions. The nuclear morphology was observed by confocal microscopy (CLSM; Olympus FV 1000 attached to an inverted microscope 1X81, Japan).

DNA fragmentation assay

C_5 treated MDA-MB-231 cells (both UV non-irradiated and irradiated) were washed twice with PBS. DNA was isolated from the cells of both the non-irradiated and irradiated groups using a quick Apoptotic DNA Ladder Detection Kit (Invitrogen), as per the manufacturer protocol. Test samples along with a 100 bp DNA marker ladder were loaded on to 1.2% agarose gel and run with 40 V for 2 h using 1XTBE buffer. DNA fragments were visualized using a UV transilluminator (UST-20M-8R, BioStep, Germany).[33]

Results and discussion

Synthesis of the coumarin–benzothiazole–chlorambucil conjugate (Cou–Benz–Cbl)

We synthesized our DDS Cou–Benz–Cbl conjugate as shown in Scheme 2. First, 7-hydroxy-4-(hydroxymethyl)-coumarin (**2**) was synthesized from 4-(bromomethyl)-7-hydroxy-coumarin (**1**) by refluxing overnight in H_2O. Next, 7-hydroxy-4-(hydroxymethyl)-coumarin and hexamine in trifluoroacetic acid (TFA) were refluxed for 2 h to yield 8-formyl-7-hydroxy-4-(hydroxymethyl)-coumarin (**3**). Later, a mixture of compound **3** and *o*-aminothiophenol in dry DMSO were heated for 1 h to afford 8-benzothiazoyl-7-hydroxyl-4-(hydroxymethyl)-coumarin (Cou–Benz–OH) (C_4). Finally, the DDS coumarin–benzothiazole–chlorambucil conjugate (Cou–Benz–Cbl) (C_5) was synthesized by coupling C_4 and the acid chloride of chlorambucil in dry DMF for 8 h. The resulting

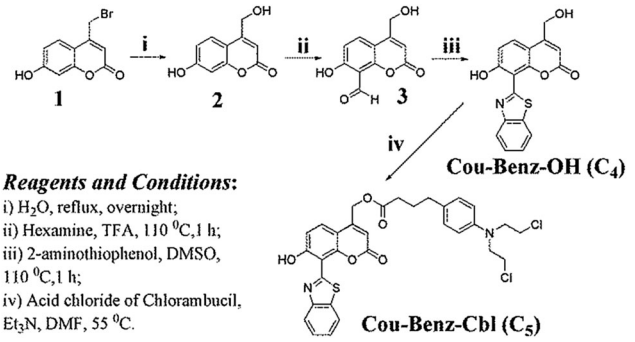

Scheme 2 Synthesis of the DDS Cou–Benz–Cbl (C_5).

DDS was characterized by UV-vis spectroscopy, FT-IR spectroscopy, NMR (^1H and ^{13}C) spectroscopy and mass spectrometry (see Fig. S1–S9, ESI†).

Photophysical properties of Cou–Benz–OH (C_4) and Cou–Benz–Cbl (C_5)

Fig. 1 shows the absorption and emission spectra of the phototrigger (C_4) and DDS (C_5) in absolute ethanol. The absorption spectrum of C_4 showed an absorption maximum at 330 nm, while the absorption spectrum of C_5 exhibited a broad range area from 200–400 nm. On the other hand, the emission spectra of C_4 and C_5 were quite similar and showed resolved dual emissions, a normal Stokes shifted emission maximum at 406 nm (enol form) along with a large Stokes shifted proton-transfer tautomer emission maximum at 516 nm (keto form). Further, the fluorescence quantum yield (Φ_f) of C_5 was calculated to be 24.27%, which is slightly higher than the parent coumarin moiety (Table S1, ESI†). The good absorbance above 350 nm and the well resolved dual emission indicate that our synthesized C_5 compound can be used for cellular imaging and light induced drug delivery in the visible wavelength region.

Solvent dependent fluorescence properties of Cou–Benz–Cbl (C_5)

It is well known that HBT can exhibit an ESIPT process upon photoexcitation and the tautomeric keto form gives a strong fluorescence emission at longer wavelength in comparison with the enol form.[34] Further, the ESIPT process exhibited by HBT is strongly dependent on the nature of the solvent. To check this, we examined the photophysical properties of Cou–Benz–Cbl (C_5) in different solvent systems. The UV-vis absorption and

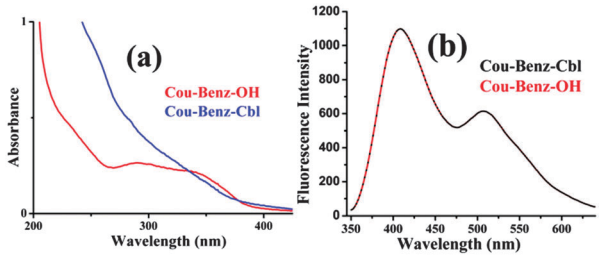

Fig. 1 The absorption (a) and emission (b) spectra of Cou–Benz–OH (C_4) and Cou–Benz–Cbl (C_5).

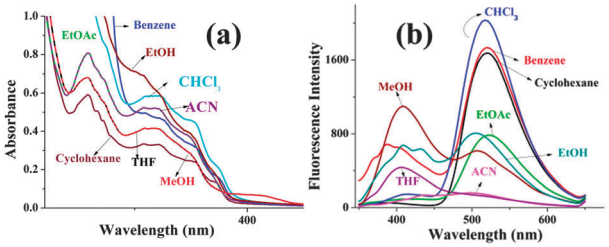

Fig. 2 (a) Absorption spectra of Cou–Benz–Cbl conjugate in different solvent system. (b) Emission spectra of Cou–Benz–Cbl ($\mathbf{C_5}$) in different solvents.

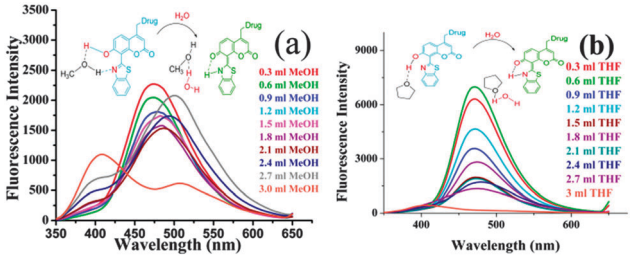

Fig. 3 Emission spectra of $\mathbf{C_5}$ in aqueous binary systems: (a) MeOH–H_2O and (b) THF–H_2O.

emission of $\mathbf{C_5}$ were recorded in different solvents at a concentration of 2×10^{-5} M.

Fig. 2b clearly shows only one emission maxima at 516 nm, corresponding to the keto form of $\mathbf{C_5}$ in non H-bonding solvents (cyclohexane, benzene and chloroform). The existence of the keto form of $\mathbf{C_5}$ in non H-bonding solvents can be attributed to ultrafast proton-transfer at intrinsically rapid rates from the hydroxyl group (–OH) of coumarin to the nitrogen atom of HBT (ESIPT). While in the case of polar aprotic solvents (ACN and THF) and polar protic solvents (EtOH and MeOH), we noted two emission maxima, one around 406 nm and another at 516 nm (keto form). The new emission maxima at 406 nm exhibited by $\mathbf{C_5}$ in H-bonding solvents corresponds to the enol form, which arises due to the restricted ESIPT process. In addition, we also noted that as we increase the H-bonding donating ability of the solvent, the intensity of the enol emission becomes stronger compared to the keto form. Moreover, no change in the UV-vis absorption of $\mathbf{C_5}$ was observed in different solvents (Fig. 2a), which indicates the presence of only one form in the ground state. We also show the naked eye colour of $\mathbf{C_5}$ in different solvents under normal conditions and a fluorescent lamp in Fig. S10 and S11, ESI†.

We have determined the lifetime of $\mathbf{C_4}$ and $\mathbf{C_5}$ in different solvents (Tables S2–S5, ESI†) from the biexponential fitting of the fluorescence decays (Fig. S12–S15, ESI†). The results revealed that as we move from benzene to THF, the lifetime of the keto form for $\mathbf{C_5}$ gradually decreases from 3.21 ns to 1.28 ns. The higher stability of the keto form in a non-polar solvent can be attributed to the decrease of the non-radiative deactivation mechanism in the excited state. On the other hand, we also noted that as we move from methanol to THF, the lifetime of the enol form corresponding to $\mathbf{C_5}$ also decreases, which may be due to the strong H-bonding ability of MeOH compared to THF. Further, the above observation was also noted for compound $\mathbf{C_4}$.

Fluorescence properties of Cou–Benz–Cbl ($\mathbf{C_5}$) in aqueous binary mixtures

To further support the presence of an ESIPT process, we studied the emission properties of $\mathbf{C_5}$ in aqueous binary mixtures of polar protic and polar aprotic solvents. In pure MeOH (polar protic solvent), $\mathbf{C_5}$ exhibited two emission bands, one with high intensity at 410 nm and another with weak intensity around 520 nm. In the case of a binary mixture of MeOH–H_2O, we observed that as we increased the percentage of water in MeOH, the strong intensity band (410 nm) corresponding to the enol form of $\mathbf{C_5}$ gradually diminished and the band at 520 nm of $\mathbf{C_5}$ corresponding to the keto form became prominent. This is mainly because the H-bond formation between MeOH and H_2O becomes more prominent over MeOH and $\mathbf{C_5}$, releasing $\mathbf{C_5}$ from the hydrogen bonding and enabling the ESIPT process (Fig. 3a). On the other hand, $\mathbf{C_5}$ exhibited only an enol emission at 400 nm in pure THF (polar aprotic solvent), which showed a red shift to 500 nm as we increased the amount of water in THF (Fig. 3b). The presence of only an enol emission at 400 nm in THF is because of the stable H-bond formation between the hydroxyl group (–OH) of $\mathbf{C_5}$ and THF that restricts the ESIPT process. With the gradual addition of water, the H-bond formation between THF and H_2O enables the ESIPT process of $\mathbf{C_5}$, leading to a keto emission at 500 nm.

pH dependent fluorescence properties of Cou–Benz–Cbl ($\mathbf{C_5}$)

As ESIPT molecules are sensitive to the pH of the medium, we studied the pH dependent emission properties of $\mathbf{C_5}$ in different pH solutions ranging from 4.4–9.4 (ACN : HEPES (30 : 70) buffer solution). Fig. 4a shows that the emission maximum of $\mathbf{C_5}$ at 527 nm undergoes a blue shift as the pH value increases from 4.4 to 9.4. Interestingly, we also observed a distinct fluorescence colour change from green to blue with the increase in the pH of the solution from acidic to basic (Fig. 4b). The above result can be attributed to the availability of the phenolic –OH of the coumarin moiety in $\mathbf{C_5}$ at different pH values. The pK_a value of the phenolic –OH of coumarin in $\mathbf{C_5}$ is around 7.4. Hence, at physiological pH and above, the phenolic –OH of the coumarin moiety remains as a phenoxide ion

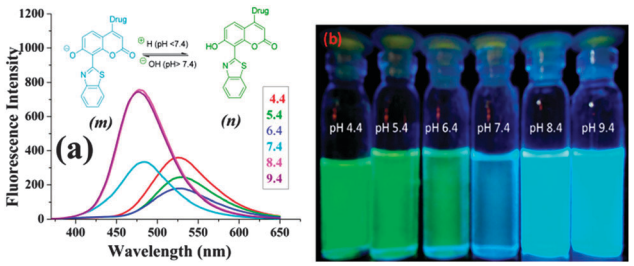

Fig. 4 (a) Emission spectra of Cou–Benz–Cbl ($\mathbf{C_5}$) at different pH values. (b) Different pH solutions of $\mathbf{C_5}$ under a fluorescent lamp.

(*m*, Fig. 4a) and the ESIPT process ceases, resulting in a blue fluorescence (λ_{max} 480 nm), as exhibited by the 7-hydroxy-coumarin moiety. While in acidic medium (pH < 7.4), the phenolic –OH of the coumarin moiety remains protonated (*n*, Fig. 4a), thus enabling the ESIPT process and resulting in a strong green fluorescence (λ_{max} 528 nm) corresponding to the keto form of $\mathbf{C_5}$.

Photochemical properties of Cou–Benz–Cbl ($\mathbf{C_5}$)

To investigate the drug release ability, Cou–Benz–Cbl ($\mathbf{C_5}$) was dissolved in MeOH : H_2O (1 : 1) and exposed to UV light (≥365 nm) using a 125 W medium pressure Hg lamp as the source with continuous stirring. The release of the anticancer drug, chlorambucil, was monitored by RP-HPLC. The HPLC results showed that as the irradiation time increased, there was a gradual decrease in the intensity of the peak at tR 8.89 min, suggesting the photocleavage of $\mathbf{C_5}$. Meanwhile, we also observed a gradual appearance of two additional new peaks at tR 6.96 min and tR 8.12 min, corresponding to the photoproducts $\mathbf{C_4}$ and chlorambucil, respectively (Fig. 5).

The light induced release of the anticancer drug was then quantified by plotting the HPLC peak area obtained for chlorambucil *vs.* different irradiation times (Fig. 6a). The photolysis was followed until 90% of chlorambucil was released by $\mathbf{C_5}$. Further, to demonstrate the precise control over the drug release by light, we monitored the release of chlorambucil by periodically switching the UV light source on and off.[35,36] Fig. 6b clearly indicates that whenever the light source was switched off, the drug release stopped, which clearly indicates that external stimulus light only induces the anticancer drug release.[37] Further, we calculated the rate constant and the photochemical quantum yield for the drug release and found the values to be $k = 1.15 \times 10^{-3}$ min^{-1} and $\Phi_p = 0.006$, respectively (Table S6, ESI†).

Cellular internalization of Cou–Benz–Cbl ($\mathbf{C_5}$)

To establish $\mathbf{C_5}$ as an efficient photoresponsive DDS, the cellular uptake capability was studied against human breast cancer cell line MDA-MB-231 using confocal microscopy (Fig. 7). After 4 h of $\mathbf{C_5}$ incubation, the images of the cell showed cyan blue fluorescence in the cytoplasm and the nucleus portion of the cell (Fig. 7D–F). At the same time, no fluorescence was observed in the control cell (Fig. 7A–C) (drug treated).

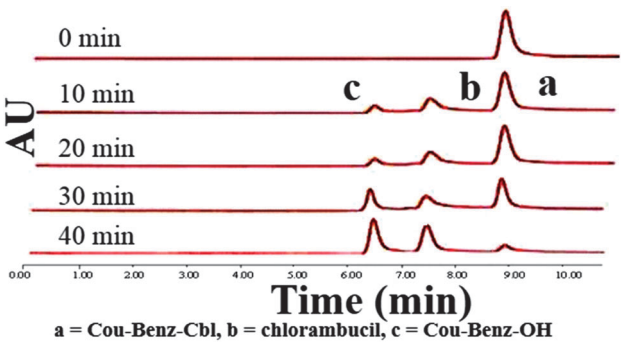

Fig. 5 (a) HPLC profile of chlorambucil release by Cou–Benz–Cbl ($\mathbf{C_5}$) using UV light (≥365 nm).

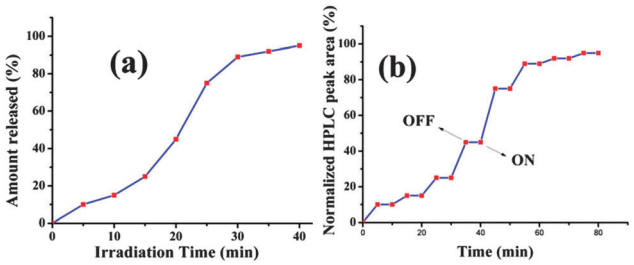

Fig. 6 (a) Amount of chlorambucil released by Cou–Benz–Cbl ($\mathbf{C_5}$) at different irradiation times using UV light (≥365 nm), (b) progress of the release of chlorambucil under bright and dark conditions (''ON'' indicates the start of UV light irradiation and ''OFF'' indicates the end of UV light irradiation.

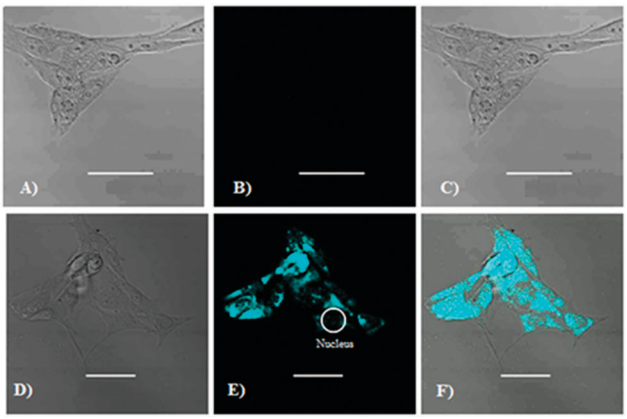

Fig. 7 Confocal images from the cellular uptake study: (A–C) control cell; (D–F) cell + Cou–Benz–Cbl ($\mathbf{C_5}$) after 4 h incubation. (A and D) bright field; (B and E) fluorescence field; (C and F) overlay images of the bright and fluorescence fields (scale bar = 50 μm).

Anticancer efficacy of $\mathbf{C_5}$ before and after UV light irradiation

The anticancer activity of $\mathbf{C_5}$ was evaluated against human breast cancer cell line MDA-MB-231 using an MTT assay. The cell viability tests of $\mathbf{C_4}$, $\mathbf{C_5}$ and chlorambucil (Cbl) (0.1–10 μg mL^{-1}) are shown in Fig. 8A (before photolysis) and Fig. 8B (after photolysis). The cytotoxicity of $\mathbf{C_5}$ was much lower than chlorambucil at any given concentration (Fig. 8A). However, after irradiation, $\mathbf{C_5}$ showed a higher cytotoxicity than free chlorambucil (Fig. 8B). This may be due to the efficient release of the anticancer drug[38] chlorambucil inside the cancer cell. On the other hand, cells incubated with Cou–Benz–OH (Fig. 8A and B) showed insignificant cell death, indicating that the photoreleased anticancer drug chlorambucil is responsible for the cytotoxicity.

Additionally, Fig. 8C and 9, corresponding to the MTT assay and fluorescence microscopy studies, revealed that cells incubated with $\mathbf{C_5}$ showed a decrease in cell viability with an increase in the irradiation time (0–30 min), confirming the controlled drug release. Further, an increased round cell population after irradiation by UV light (≥365 nm) for 30 min

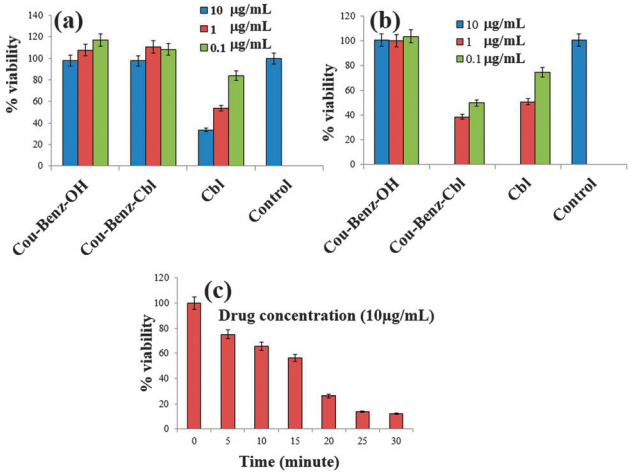

Fig. 8 The cell viability studies of Cou–Benz–OH, Cou–Benz–Cbl conjugate and Cbl (0.1–10 μg mL^{-1}) was depicted (a) before photolysis; and (b) after photolysis; (c) cell viability test of Cou–Benz–Cbl conjugate (10 μM mL^{-1}), at regular time intervals of irradiation.

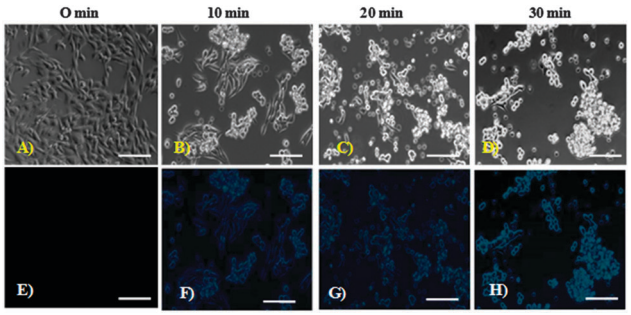

Fig. 9 Anticancer activity study of Cou–Benz–Cbl (C_5) by fluorescence microscopy: (A and E) control cell; (B and F) after 10 min of UV irradiation; (C and G) after 20 min of UV irradiation; (D and H) after 30 min of UV irradiation. (A–D) Bright field and (E–H) fluorescence field (scale bar = 100 μm).

indicates cell death (Fig. 9D and H). The higher cytotoxicity of C_5 compared to free chlorambucil after UV light irradiation suggests that C_5 can enhance the efficiency of the intracellular delivery of the drug chlorambucil for a sustained period of time.

Apoptosis induction by Cou–Benz–Cbl (C_5)

To investigate whether the photoinduced cytotoxicity of C_5 in MDA-MB-231 cells proceeds through an apoptotic mechanism, a cell and nuclear morphological study was carried out by SEM and PI staining. The SEM images (Fig. 10A–F) show morphological changes in the MDA-MB-231 cells. The control cells have a spindle shape with intact cell membranes (Fig. 10A–C). In contrast, the images of the cells incubated with C_5 after UV treatment exhibit a significant loss in the membrane rigidity and show deformation of the cell with membrane blebbing, a characteristic feature of apoptotic cell death (Fig. 10D–F).

Fig. 10G and H show the nuclear morphology upon drug treatment before (smooth) and after (condensed or fragmented) photolysis, which are easily distinguished microscopically.

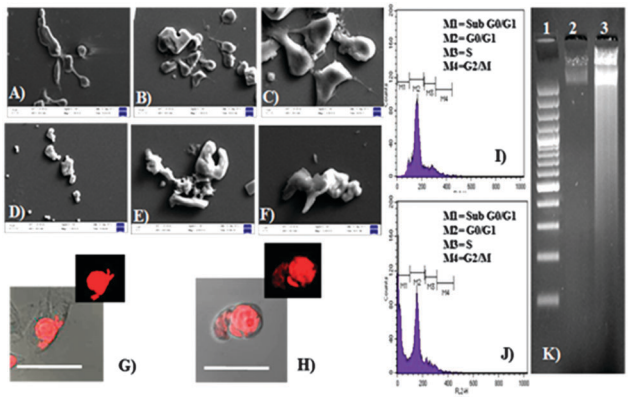

Fig. 10 Cell apoptosis study: (A–C) SEM images of the control cell; (D–F) SEM images of the treated cell (30 min irradiation); PI staining of (G) the control cell and (H) the treated cell; cell cycle analysis by FACS (I) before irradiation and (J) after irradiation; (K) DNA fragmentation assay. Scale bars = 50 μm.

The nuclear morphology analysis by PI staining showed characteristic apoptotic changes, like nuclear fragmentation, in the breast cancer cells after treatment for 48 h by UV irradiation with C_5 (Fig. 10H) in comparison to cells before UV treatment (Fig. 10G). For further confirmation of apoptotic cell death by DNA damage, a DNA fragmentation assay was performed (Fig. 10K). Apoptosis by DNA fragmentation can appear in two patterns on an agarose gel: as a ''DNA ladder'' because of endonucleases and/or as a ''smear'' of randomly degraded DNA molecules. DNA agarose gel electrophoresis demonstrated that the MDA-MB-231 cells displayed DNA smears for apoptosis after UV treatment (Fig. 10K; lane 3). No DNA fragmentation was observed in the control cells (Fig. 10K; lane 2).

C_5 induced apoptosis in MDA-MB-231 cells was also demonstrated by fluorescence-activated cell sorting (FACS). As shown in Fig. 10I and J, 1.74% sub-G0/G1, 95.21% G0/G1, 0.67% S and 2.46% G2/M phase cells were found in the non-irradiated drug treated control (Fig. 10I), whereas the UV irradiated drug treated cells (Fig. 10J) had 21.79% sub-G0/G1, 61.36% G0/G1, 12.78% S, and 2.87% G2/M phase cells after 48 h of incubation. A rise in the sub G0/G1 cell population is indicative of apoptotic cell death, which was clearly observed in the UV irradiated C_5 treated cells (Fig. 10J). In conclusion, C_5 upon irradiation releases a drug of interest, which induces an arrest in the G2/M phase of the cell cycle with an instantaneous increase in the sub-G0/G1phase of the cells and a decrease in the G0/G1 phase of the cells.

Conclusion

In conclusion, we have successfully synthesized Cou–Benz–Cbl conjugate (C_5), an ESIPT based drug delivery system. Our newly synthesised DDS showed a large Stokes shift, by which it can avoid self-absorption. The photophysical properties revealed that our DDS is highly sensitive to the environment, in particular towards the polarity of the solvent and pH of the medium.

Our DDS efficiently released the anticancer drug chlorambucil upon irradiation using UV-light ($\geq$365 nm). *In vitro* studies showed that our DDS can act both as a cell imaging agent due to its high fluorescence nature and a phototrigger for controlled drug release upon UV light irradiation. In the future, we would like to explore the *in vivo* behaviour of this prepared DDS.

Acknowledgements

We thank the DST (SERB) for financial support and the DST-FIST for 400 MHz NMR spectroscopy. S. Barman, S. K. Mukhopadhyay, and M. Gangopadhyay are grateful to the Indian Institute of Technology Kharagpur, and S. Biswas is grateful to the UGC (India) for their research fellowships.

Notes and references

1 N. C. Fan, F. Y. Chenge, J. A. Ho and C. S. Yeh, *Angew. Chem., Int. Ed.*, 2012, **51**, 35.
2 T. Nagasaki, A. Taniguchi and S. Tamagaki, *Bioconjugate Chem.*, 2003, **14**, 513–516.
3 W. Lin, L. Long and W. Tan, *Chem. Commun.*, 2010, **46**, 1503–1505.
4 J. Liu, Y. Sun, H. Zhang, Y. Huo, Y. Shi, H. Shi and W. Guo, *RSC Adv.*, 2014, **4**, 64542–64550.
5 A. S. Vasylevska, A. A. Karasyov, S. M. Borisov and C. Krause, *Anal. Bioanal. Chem.*, 2007, **387**, 2131–2141.
6 J. Keck, H. E. A. Kramer, H. Port, T. Hirsch, P. Fischer and G. Rytz, *J. Phys. Chem.*, 1996, **100**, 14468–14475.
7 J. Pospisil and S. Nespurek, *Prog. Polym. Sci.*, 2000, **25**, 1261–1335.
8 K. Y. Chen, C. C. Hsieh, Y. M. Cheng, C. H. Lai and P. T. Chou, *Chem. Commun.*, 2006, 4395–4397.
9 Y. Zhang, J. Wang, W. Zheng, T. Chen, Q. Tong and D. Li, *J. Mater. Chem. B*, 2014, **2**, 4159.
10 M. B. Cardoso, D. Samios, N. P. Silveira, F. S. Rodembusch and V. Stefani, *Photochem. Photobiol. Sci.*, 2007, **6**, 99–102.
11 S. Goswami, A. Manna, S. Paul, A. K. Das, K. Aich and P. K. Nandi, *Chem. Commun.*, 2013, **49**, 2912–2914.
12 S. Goswami, A. Manna, S. Paul, A. K. Maity, P. Saha, C. K. Quah and H. K. Fun, *RSC Adv.*, 2014, **4**, 34572–34576.
13 S. Goswami, A. Manna, M. Mondal and D. Sarkar, *RSC Adv.*, 2014, **4**, 62639–62643.
14 S. Goswami, A. Manna, S. Paul, A. K. Das, P. K. Nandi, A. K. Maity and P. Saha, *Tetrahedron Lett.*, 2014, **55**, 490–494.
15 T. Mutai, H. Sawatani, T. Shida, H. Shono and K. Araki, *J. Org. Chem.*, 2013, **78**, 2482–2489.
16 H. Esisenberger, B. Nickle, A. A. Ruth, W. Al-Soufi, K. H. Grellmann and M. Novo, *J. Phys. Chem.*, 1991, **95**, 10509–10518.
17 V. S. Patil, V. S. Padalkar, K. R. Phatangare, V. D. Gupta, P. G. Umape and N. Sekar, *J. Phys. Chem. A*, 2012, **116**, 536–545.
18 A. J. G. Strandjord and P. F. Barbara, *J. Phys. Chem.*, 1985, **89**, 2355–2361.
19 P. Majumdar and J. Zhao, *J. Phys. Chem. B*, 2015, **119**, 2384.
20 R. S. Becker, C. Lenoble and A. Zein, *J. Phys. Chem.*, 1987, **91**, 3509–3511.
21 S. Liua, L. Zhang, W. Zanc, X. Yaoc, Y. Yanga and X. Liua, *Sens. Actuators, B*, 2014, **192**, 386–392.
22 J. E. Kwon and S. Y. Park, *Adv. Mater.*, 2011, **23**, 3615–3642.
23 M. J. Kwak and Y. Kim, *Bull. Korean Chem. Soc.*, 2009, **30**, 2865.
24 K. Sakai, T. Tsuzuki, Y. Itoh, M. Ichikawa and Y. Taniguchi, *Appl. Phys. Lett.*, 2005, **86**, 081103.
25 S. Park, S. Kim, J. Seo and S. Y. Park, *Macromol. Res.*, 2008, **16**, 385–395.
26 P. G. Parejo, M. Zayata and D. J. Levy, *J. Mater. Chem.*, 2006, **16**, 2165–2169.
27 K. Zheng, W. Lin, L. Tan, H. Chena and H. Cuia, *Chem. Sci.*, 2014, **5**, 3439.
28 Y. H. Kim, S. G. Roh, S. D. Jung, M. A. Chung, H. K. Kim and D. W. Cho, *Photochem. Photobiol. Sci.*, 2010, **9**, 722–729.
29 P. Brerbon, Q. Peng, G. Ferrandi, C. Stauffacher, O. Wiest and P. Helquist, *J. Org. Chem.*, 2012, **77**, 2756–2762.
30 T. Mosmann, *J. Immunol. Methods*, 1983, **65**, 55–63.
31 M. Pilatova, L. Varinska, P. Periesi, M. Sarissky, L. Mirossay, P. Solar, A. Ostro and J. Moizis, *Toxicol. in Vitro*, 2010, **24**, 1347–1355.
32 Y. M. Shon, K. H. Lee, S. J. Goerss, I. Y. Kim, C. Kimble, J. J. V. Gompel, K. Bennet, C. D. Blaha and S. Y. Chang, *Neurosci. Lett.*, 2010, **475**, 136–140.
33 A. H. Wyllie, J. F. Kerr and A. R. Currie, *Int. Rev. Cytol.*, 1980, **68**, 251–306.
34 L. Xie, Y. Chen, W. Wu, H. Guo, J. Zhao and X. Yu, *Dyes Pigm.*, 2012, **92**, 1361–1369.
35 S. Karthik, B. Saha, S. K. Ghosh and N. D. P. Singh, *Chem. Commun.*, 2013, **49**, 10471–10473.
36 A. Jana, K. S. P. Devi, T. K. Maiti and N. D. P. Singh, *J. Am. Chem. Soc.*, 2012, **134**, 7656–7659.
37 S. Barman, S. K. Mukhopadhyay, K. K. Behara, S. Dey and N. D. P. Singh, *ACS Appl. Mater. Interfaces*, 2014, **6**, 7045–7054.
38 M. Ikbal, B. Saha, S. Barman, S. Atta, D. Banerjee, S. Ghosh and N. D. P. Singh, *Org. Biomol. Chem.*, 2014, **12**, 3459–3469.